Supplemental data belonging to "High resolution analysis of epigenetic changes associated with X inactivation" (Marks et al., Genome Research, 2009)

Supplemental results

Validation of differentiation (and XCI) of LF2 and E14 cells

Undifferentiated LF2 and E14 ES cells were treated with *all-trans*-retinoic acid (atRA) for 4 days or grown to embryoid bodies (EBs) for 10 days. RT-qPCR analysis showed a 10-100 fold drop in expression of the stem cell specific genes *Oct4 (Pou5f1)*, *Nanog* and *Rex1* (*Zfp42*) after 4d atRA treatment or EB formation, while expression of the differentiation specific genes *Sox9*, *Gata6* and *Hoxa1* was 10-100 fold upregulated (Fig S1a). Concerning XCI, RT-qPCR confirmed the decreased *Tsix* expression (~10 fold) after 4d atRA treatment in LF2 and E14 cells (Fig S1b), accompanied by (high) expression of *Xist* in LF2 cells. For the LF2 EBs, RNA fluorescent in situ hybridization (RNA FISH) showed that 81% of the cells showed a dense *Xist* staining, indicating that a significant number of LF2 cells started XCI. The undifferentiated cells, 4d atRA treated cells as well as the EBs, were subsequently prepared for ChIP-Chip. An overview of the antibodies used in ChIP-chip (and ChIP-Seq) is shown in Supplemental Table 2.

ChIP-Seq analysis for the LF2 cells

Distribution H3K27me3 during differentiation over autosomes

Except for chromosome X, we observed some remarkable differences in the amount of autosomal H3K27me3 between E14 and LF2 cells, of which the three major differences occur on chromosomes 6, 8 and 11 (Fig S7a). The higher amount of H3K27me3 on chromosomes 6 and 11 in E14 as compared to LF2 (for both 9%) is mostly localized over the Hox clusters on these chromosomes and probably represents a slight difference in differentiation status of these cells after EB formation. The higher amount of H3K27me3 on chromosome 8 in LF2 cells as compared to E14 cells (13%) is most likely caused by an interchromosomal conversion between chromosome 8 and chromosome X present in the LF2 cells (discussed below).

Detection of chromosomal abnormalities in E14, LF2 and XT67E1 cells

While the XT67E1 cells show a chromosome-wide increase of H3K27me3 during EB formation on the X chromosome (Fig 5a & b), the increase of H3K27me3 in LF2 cells is only observed in the proximal part of the X chromosome (~0-109 Mb), not in the distal part (~109-167 Mb) (Fig S8). As female mouse ES cells are well known for their genetic instability (Nichols et al., 1990; Liu et al., 1997; Sugawara et al., 2006; Silva et al., 2008), we analyzed chromosomal abnormalities using our ChIP-Seq data to further investigate the discrepancy between the LF2 and XT67E1 cells.

To detect chromosomal differences between E14, LF2 and XT67E1 cells, the number of tags obtained in the H3K27me3 ChIP-Seq experiments was normalized to the length of the individual chromosomes (Fig S9a). The relative low number of tags mapped on chromosome X as compared to autosomes is due to the high abundance of repeats present on chromosome X, which reduces the number of tags that can be mapped specifically. The low number of tags mapped on chromosome X in E14 cells

as compared to LF2 and XT67E1 cells is explained by the fact that the tags in E14 cells originate from its single X chromosome, while in LF2 and XT67E1 cells they are obtained from both X chromosomes. The relatively high number of tags mapped to chromosome 2, 6 and 11 in all cells (Fig S9a) can be explained by the presence of Hox clusters on these chromosomes, which are heavily decorated with H3K27me3.

Considering the E14 and LF2 cells, the only chromosome that showed a > 10% difference in number of tags next to chromosome X is chromosome 8 (Fig S9a). In contrast to the situation in E14 cells, this chromosome contained 26% more tags than expected on its size in the LF2 cells, suggesting that part of chromosome 8 might be duplicated in these cells. The H3K27me3 ChIP-Seq profiles over chromosome 8 (Fig S9b) show that the differential tags in the LF2 cells as compared to the E14 cells are mainly located to the distal part of the chromosome, suggesting that this part of chromosome 8 is trisomic in at least a subpopulation of the undifferentiated LF2 cells used for this study. This is in line with previous reports, which show that (partial) trisomy of chromosome 8 is a common phenomenon in mouse ES cells (Liu et al., 1997; Sugawara et al., 2006). Next to the partial trisomy of chromosome 8, we also observed a remarkable LF2 specific increase of 11% of H3K27me3 on chromosome 8 during EB formation (Fig S7a). The increase is specifically localized over the distal part of the chromosome (Fig S9c), exactly at the part that was shown to be trisomic (Fig S9b). Together with the observation that the distal part (~109-167 Mb) of the Xi in the LF2 cells did not show an increase in H3K27me3 (Fig S8), this suggested an interchromosomal conversion between chromosome 8 and chromosome X present in at least a subpopulation of the LF2 cells used for this study. RNA/DNA FISH paintings for chromosome 8, chromosome X and *Xist* indeed showed that 84% of the LF2 10d EBs contained three clear signals for chromosome 8, of which the smallest colocalized with the Xi, as visualized by chromosome X or *Xist* stainings (Fig S10). This strongly suggests that one of the two X chromosomes in these LF2 cells is a mosaic of the proximal part of the X chromosome (~0-109 Mb) and the distal part of chromosome 8 (~80-133 Mb). Still containing the *Xist* locus, the X chromosomal part of this mosaic X;8 chromosome was inactivated during differentiation. This is most probably the reason why we did not observe an increase in H3K27me3 at the distal part of chromosome X in the LF2 cells after EB formation (Fig S8). Further DNA FISH studies suggest that the increase in H3K27me3 sequence tags over the trisomic part of chromosome 8 during XCI is the result of a positive selection for a minority of LF2 cells containing the interchromosomal conversion X;8 during EB formation (data not shown). We can however not exclude that the increase is also partly caused by increased levels of H3K27me3 over the X-chromosomal translocated part of chromosome 8.

Considering the XT67E1 cells, the tag distributions over the chromosomes are very similar to the LF2 cells (Fig S9a). A comparison with the E14 cells shows that the XT67E1 cells are fully trisomic for chromosome 8 (Fig S9d).

Supplemental figure legends

Supplemental figure 1

Gene expression profiles of a selected panel of genes involved in development or XCI in E14 and LF2 cells, as determined by RT-qPCR. (undiff: undifferentiated)

Fig S1a: Gene expression of E14 and LF2 cells showing clear differentiation after 4d atRA treatment or 10d EB formation.

Fig S1b: *Tsix* and *Xist* expression in LF2 and E14 cells after 4d atRA treatment. Expression levels of both genes were determined by expression profiling of two different exons (PCR amplicons shown in Fig 1b), giving similar results. The E14 *Xist* expression levels were below background (-RT control) and therefore not included in the figure.

Supplemental figure 2

Fig S2a: Overview of the epigenetic landscape and expression of the *Slc16a2* gene on chromosome X in female LF2 and male E14 ES cells during differentiation as profiled by ChIP-chip. Genes as well as direction of transcription are indicated below all profiles. For further details, see Figure 1.

Fig S2b: Validation of the expression profile shown in Fig S2a. *Slc16a2* gene expression in LF2 cells during XCI as determined by RT-qPCR, showing clear upregulation of *Slc16a2* after 4d atRA treatment similar to the expression profile in Fig S2a. The male E14 cells showed constitutive expression of *Slc16a2* at all three differentiation stages. Primers used for PCR (Supplemental Table 1) are intron-spanning to avoid background signals of genomic DNA.

Supplemental figure 3

Late inactivation of *Atrx* after the onset of XCI. RNA FISH for *Atrx* (red) and *Xist* (green) in LF2 cells during XCI (using atRA differentiation for indicated number of days). DNA is stained with DAPI. *Atrx* is biallelic expressed in undifferentiated LF2 cells, as well as after 2d and 4d atRA treatment of these cells (represented by two red dots). *Atrx* expression becomes monoallelic at 8 days atRA treatment (only one red dot). Genes showing regular XCI such as *Pgk* show already monoallelic expression at 4 days atRA treatment (data not shown).

Supplemental figure 4

Overview of the epigenetic landscape and expression of the genes *Pgk1* (Fig S4a), *Atrx* (Fig S4b) and *Gdpd2* (Fig S4c) on chromosome X in female LF2 and male E14 ES cells during differentiation as profiled by ChIP-chip. Genes as well as direction of transcription are indicated below all profiles. For further details, see Figure 1.

Supplemental figure 5

Field of female XT67E1 ES cells showing the kinetics of XCI. *Xist* RNA FISH (green) is combined with IF for H3K27me3 (red). DNA is stained with DAPI (blue). The images at the undifferentiated stage are maximum intensity projections (60 Z-sections, 0.2uM step size) which allows the visualization of the Xist pinpoints from both active X chromosomes. All other images are single Z-sections. The percentage of nuclei in which stainings were observed is indicated. Cells with H3K27me3 accumulation at the Xi, but no *Xist*, were not observed.

Supplemental figure 6

Examples of H3K27me3 and H3K4me3 ChIP-Seq profiles of XT67E1, LF2 and E14 cells on chromosome X. Comparisons of the ChIP-Seq and ChIP-chip data (Fig S6b & S6c). Annotation is provided above each individual track.

Fig S6a: H3K27me3 ChIP-Seq profile (XT67E1, LF2 and E14 cells) over the *Arx* gene on chromosome X.

Fig S6b: H3K27me3 ChIP-Seq (XT67E1 cells) and ChIP-chip (LF2 cells) profile over the *Ar* gene on chromosome X.

Fig S6c: H3K4me3 ChIP-Seq (XT67E1 cells) and ChIP-chip (LF2 cells) profile over the *Pin4* and *Ercc6l* gene on chromosome X.

Supplemental figure 7

Specific enrichment of H3K27me3 on the X chromosome after 10d EB formation in mouse female XT67E1 and LF2 ES cells, but not in male E14 ES cells.

Fig S7a: H3K27me3 tag distribution (representing amounts of H3K27me3) over the chromosomes in XT67E1 E14 or LF2 cells (ratio of 4d atRA or 10d EB versus undifferentiated cells in %).

Fig S7b: H3K4me3 tag distribution (representing amounts of H3K4me3) over the chromosomes in XT67E1 cells (ratio of 4d atRA or 10d EB versus undifferentiated cells in %).

Supplemental Figure 8

Kinetics of H3K27me3 over chromosome X during XCI in LF2 cells. Upper panel: H3K27me3 profiles over chromosome X in LF2 cells. Chromosome X is subdivided in bins of 1 Mb, followed by counting of the number of tags per bin; Lower panel: Subtraction track of the profiles shown in the upper panel at a higher resolution (100 kb bins). For further details, see Figure 5.

Supplemental figure 9

Chromosomal abnormalities in LF2, E14 or XT67E1 cells.

Fig S9a: Amount of H3K27me3 tags relative to chromosome size in undifferentiated LF2, XT67E1 and E14 cells.

Fig S9b: H3K27me3 profiles over chromosome 8 in LF2 and E14 undifferentiated cells to show that the distal part is trisomic in LF2 cells. Chromosome 8 was subdivided in bins of 1 Mb, followed by counting of the number of tags per bin.

Fig S9c: H3K27me3 profiles over chromosome 8 in LF2 undifferentiated cells and LF2 10d EBs showing the increase only in the distal part chromosome 8 during EB formation. For details see Fig S9b.

Fig S9d: H3K27me3 profiles over chromosome 8 in E14 and XT67E1 undifferentiated cells to show that the complete chromosome is trisomic in XT67E1 cells. For details see Fig S9b.

Supplemental figure 10

Fig S10: *Xist* RNA FISH combined with DNA FISH specific for chromosome 8 or chromosome X after 10d EB formation of LF2 cells. DNA is stained with DAPI (blue) in the left picture. Other color-coding is indicated below the pictures. The Xi (with chromosome 8) and Xa, as based on *Xist* staining, is indicated in the second picture. This staining pattern shown was observed in 47 of 56 nuclei (84%).

Supplemental figure 11
H3K27me3 ChIP-Seq profile of XT67E1 cells over the *Meis2* gene on chromosome 2, one of the five autosomal H3K27me3 regions showing a strong decrease of H3K27me3 after 4d atRA treatment. Annotation is provided above each individual track.

Supplemental tables

Supplemental table 1: Overview of primers used for RT-qPCR

Gene	Primer name	Sequence (5'- 3')	MM9 coordinates	Bp size PCR
Gapdh	Gapdh-qRT-F	TTCACCACCATGGAGAAGGC	chr10:121,606,715-121,606,734*	52
	Gapdh-qRT-R	CCCTTTTGGCTCCACCCT	chr10:121,606,749-121,606,766*	
b-actin	Actin-qRT-F	AGTGTGACGTTGACATCCGT	chr5:143,665,760-143,665,779	120
	Actin-qRT-R	TGCTAGGAGCCAGAGCAGTA	chr5:143,665,860-143,665,879	
Tubulin	Tubulin-qRT-F	GCACTCTGATTGTGCCTTCA	chr2:151,285,277-151,285,296*	202
	Tubulin-qRT-R	AGGGTAGGGTACCAGGTTGG	chr2:151,285,459-151,285,478*	
Oct4	Oct4-qRT-F	TTGAGAACCGTGTGAGGTGG	chr17:35,646,978-35,646,997	51
	Oct4-qRT-R	TCGGGCACTTCAGAAACATG	chr17:35,647,029-35,647,028	
Nanog	Nanog-qRT-F	AGCAGAAGATGCGGACTGTGTT	chr6:122,661,691-122,661,712	51
	Nanog-qRT-R	CCTTGAGTGCACACAGCTGG	chr6:122,661,722-122,661,741	
Rex1	Rex1-qRT-F	AGGCCAGTCCAGAATACCAG	chr8:44,381,595-44,381,614	111
	Rex1-qRT-R	TAGGTATCCGTCAGGGAAGC	chr8:44,381,686-44,381,705	
Sox9	Sox9-qRT-F	CCTTCAGAGTTAACATGGAGGACG	chr11:112,647,141-112,647,164	51
	Sox9-qRT-R	TCCAAACAGGCAGGGAGATT	chr11:112,647,172-112,647,191	
Gata6	Gata6-qRT-F	GAGCTGGTGCTACCAAGAGG	chr18:11,084,479-11,084,498	193
	Gata6-qRT-R	TGCAAAAGCCCATCTCTTCT	chr18:11,084,652-11,084,671	
Hoxa1	Hoxa1-qRT-F	TCCTGCAAATGTCTGATGGC	chr6:52,106,393-52,106,412	51
	Hoxa1-qRT-R	GATGTCGGCTGGAGAACAGTTAGT	chr6:52,106,420-52,106,443	
Tsix exon 1	Tsix-ex1-qRT-F	TACCTGCAAGCGCTACACAC	chrX:100,643,145-100,643,164	142
	Tsix-ex1-qRT-R	GCTGGCTATCACGCTCTTCT	chrX:100,643,267-100,643,286	
Tsix exon 4	Tsix-ex4-qRT-F	CGACCTCAGATGAGGAGAGG	chrX:100,678,940-100,678,959	96
	Tsix-ex4-qRT-R	CCTCCAAATCGGTCACAACT	chrX:100,679,016-100,679,035	
Xist exon 1	Xist-ex1-qRT-F	GCCAACCAATGAGACCACTT	chrX:100,673,010-100,673,029	129
	Xist-ex1-qRT-R	TTCTCTCAAACCACCACACG	chrX:100,673,119-100,673,138	
Xist exon 7	Xist-ex7-qRT-F	CTTTGGGCTTAGGTGAGCAG	chrX:100,660,941-100,660,960	123
	Xist-ex7-qRT-R	CCAGGAGTTCCTTTGGTGAA	chrX:100,661,044-100,661,063	
Slc16a2 exon 3/4	Slc-ex3/4-qRT-F	TGGTTACTTCGTCCCCTACG	chrX:100,903,102-100,903,121	150
	Slc-ex3/4-qRT-R	CCAGGGATGGAGTCACTGAT	chrX:100,901,613-100,901,632	
Slc16a2 exon 4/5	Slc-ex4/5-qRT-F	CAGTGACTCCATCCCTGGAC	chrX:100,901,611-100,901,630	90
	Slc-ex4/5-qRT-R	CATAGGGGGATCATCATGGA	chrX:100,897,010-100,897,029	

*among others

Supplemental table 2: Overview of antibodies used for ChIP-chip or ChIP-Seq experiments

Modification	Antibody cat#	Antibody lot#	Type	Supplier	Amount per ChIP
H3K4me3	pAb-MEHAHS-024	HC-0010	polycl	Diagenode	2 μg
H3K36me3	CS-058-100	A114-001	polycl	Diagenode	2 μg
H3K27me3*			polycl		6 μg
H3K9me2*			polycl		8 μg
H3Core	ab1791-100	237566	polycl	Abcam	2 μg
TBP	mAb-TBPCSH-100	DA-0010	monocl	Diagenode	2 μg
RNAPII	AC-055-100	001	monocl	Diagenode	2 μg
*These antibodies were a kind gift of Thomas Jenuwein; they are similar to the following antibodies:					
H3K27me3	07-449	6523	polycl	Upstate/Millip	6 μg
H3K9me2	07-441	4677	polycl	Upstate/Millip	8 μg

Supplemental references

Liu, X., H. Wu, J. Loring, S. Hormuzdi, C.M. Disteche, P. Bornstein, and R. Jaenisch. 1997. Trisomy eight in ES cells is a common potential problem in gene targeting and interferes with germ line transmission. *Dev Dyn* **209:** 85-91.

Nichols, J., E.P. Evans, and A.G. Smith. 1990. Establishment of germ-line-competent embryonic stem (ES) cells using differentiation inhibiting activity. *Development* **110:** 1341-1348.

Silva, S.S., R.K. Rowntree, S. Mekhoubad, and J.T. Lee. 2008. X-chromosome inactivation and epigenetic fluidity in human embryonic stem cells. *Proc Natl Acad Sci U S A* **105:** 4820-4825.

Sugawara, A., K. Goto, Y. Sotomaru, T. Sofuni, and T. Ito. 2006. Current status of chromosomal abnormalities in mouse embryonic stem cell lines used in Japan. *Comp Med* **56:** 31-34.

Supplemental figure 1

Fig S1a

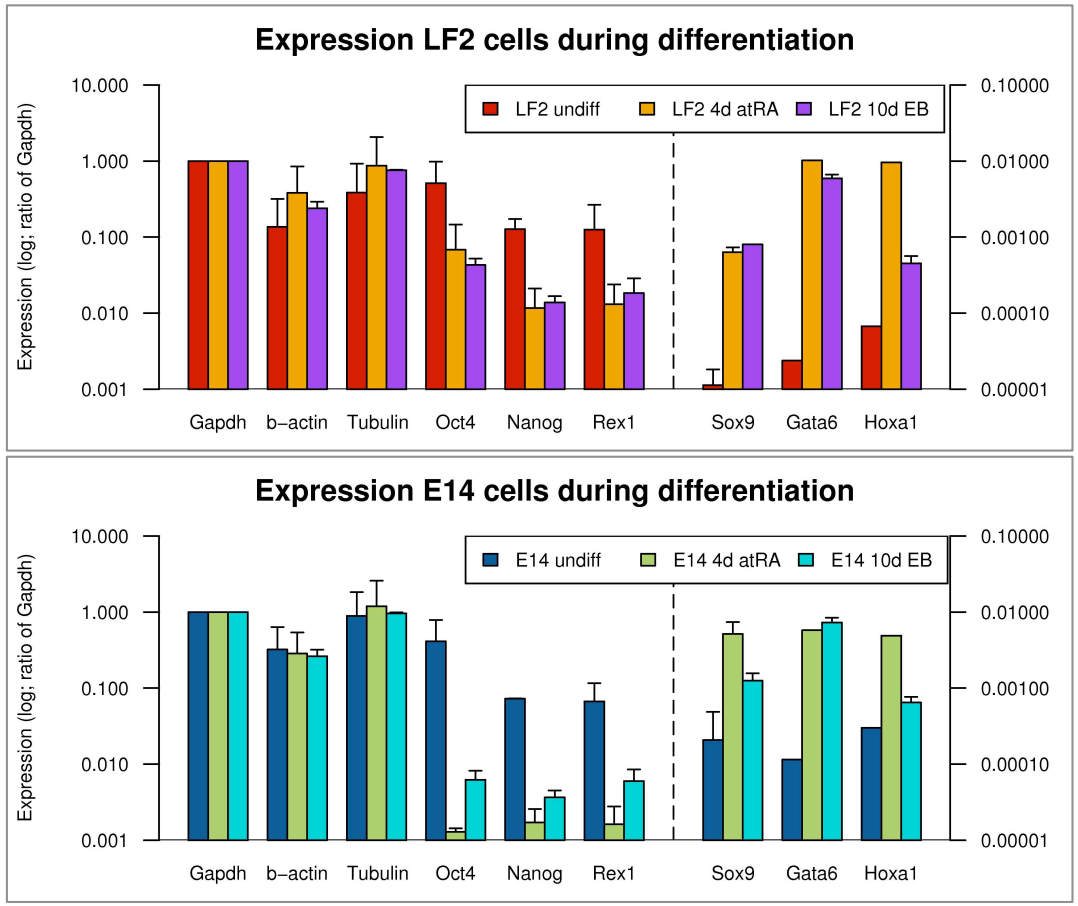

Fig S1b

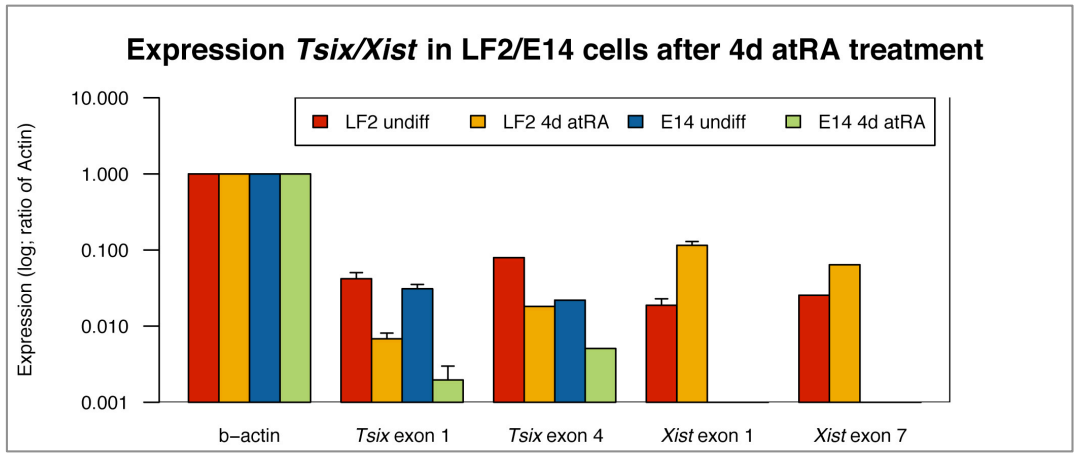

Supplemental figure 2

Fig S2a

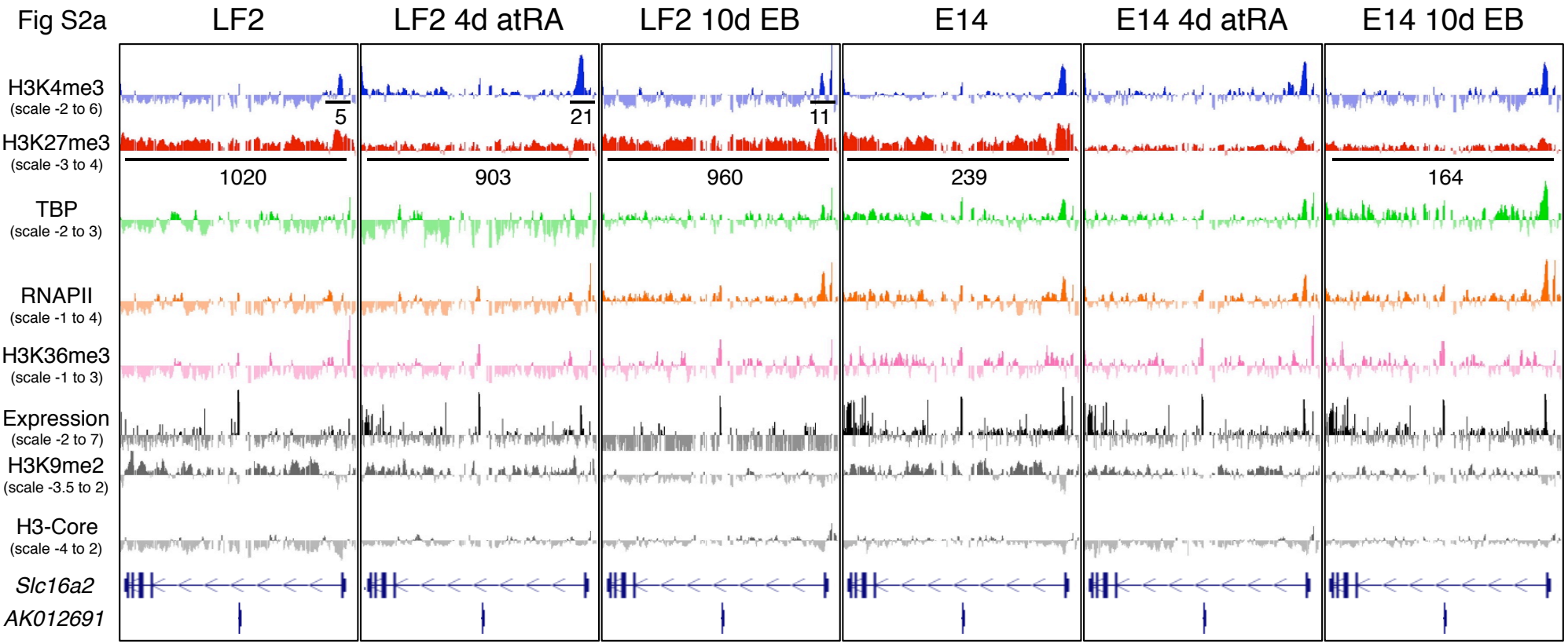

Fig S2b

Supplemental figure 3

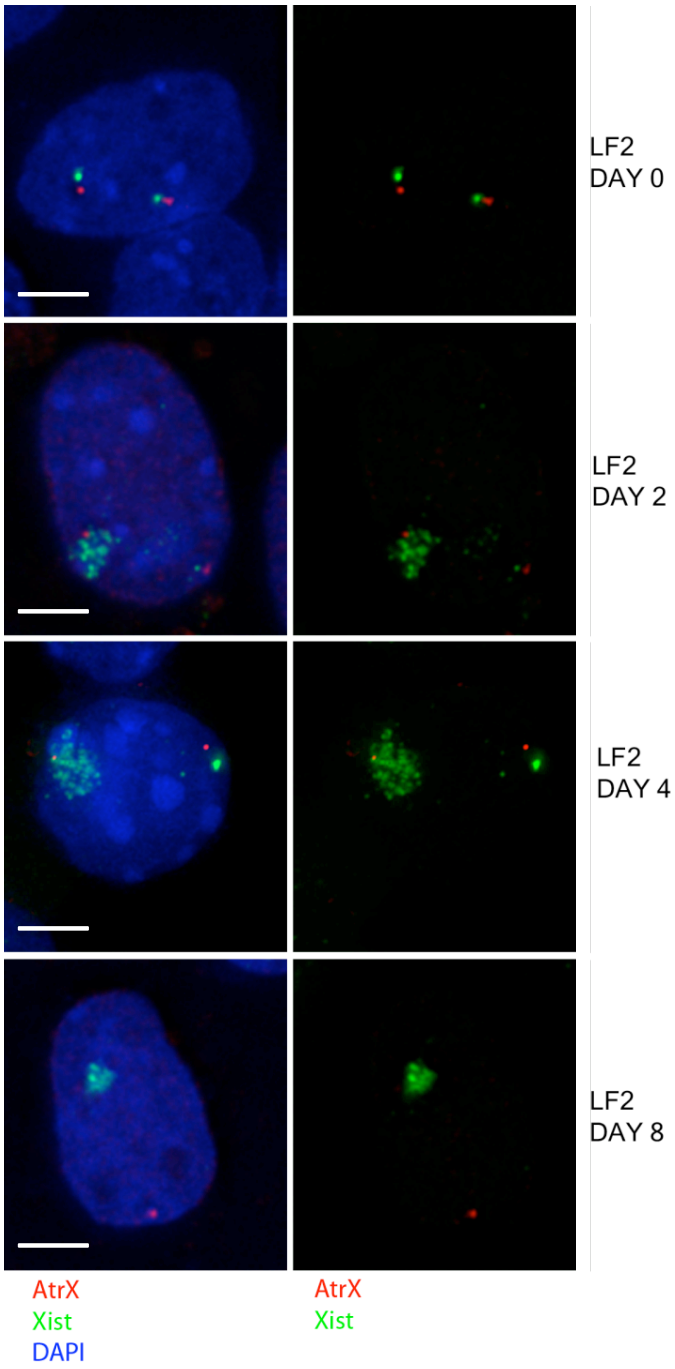

Supplemental figure 4

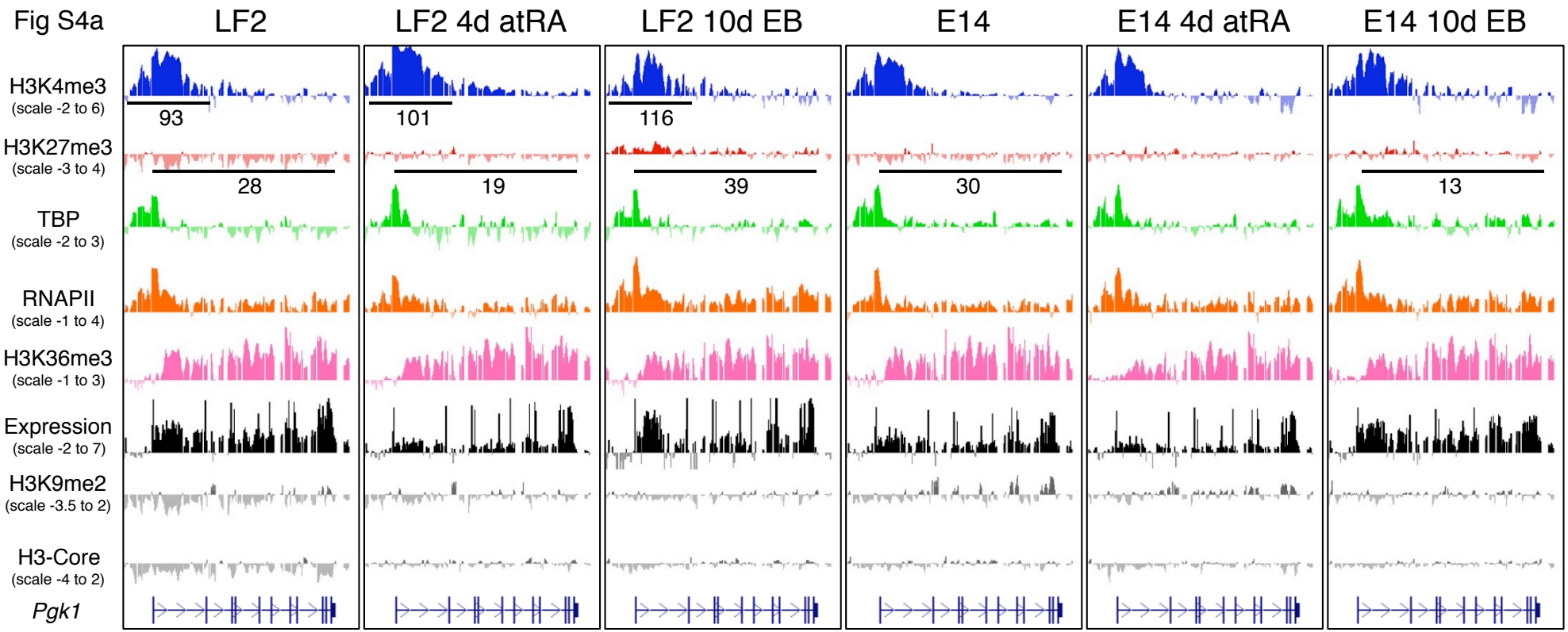

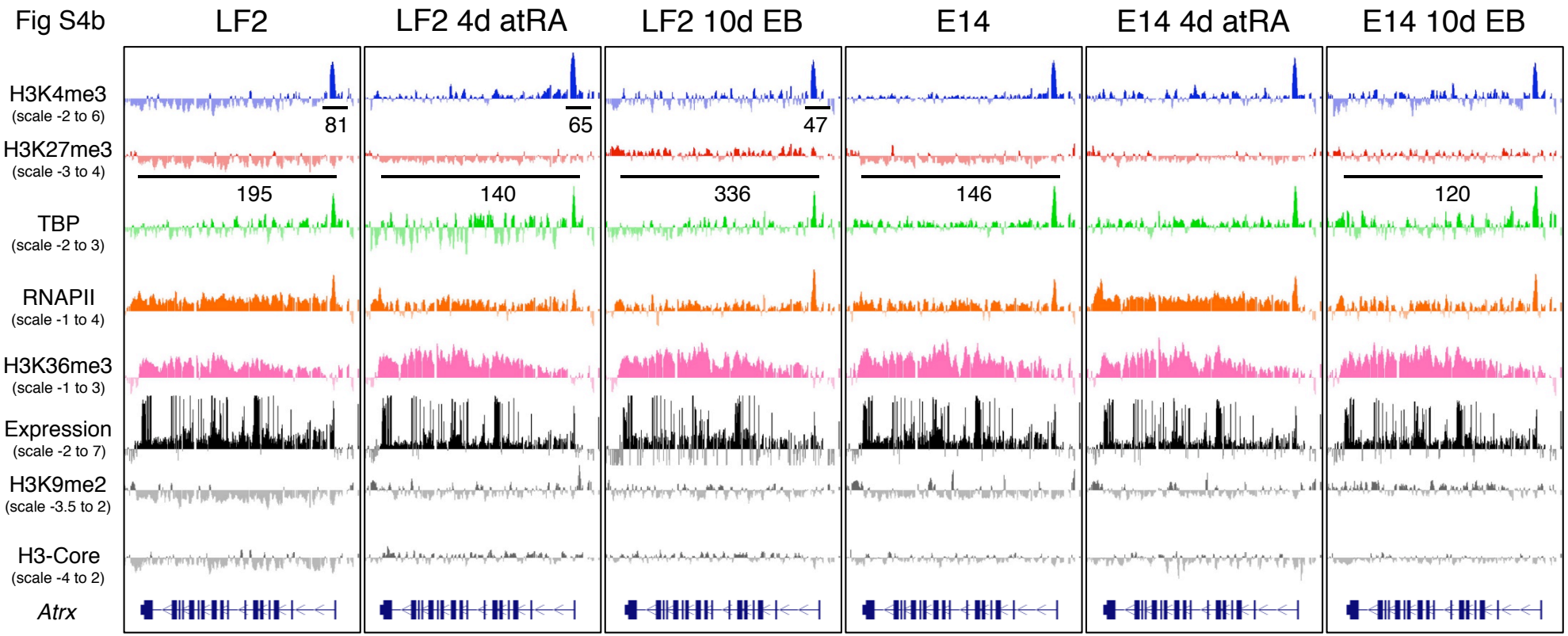
Fig S4b
LF2
LF2 4d atRA
LF2 10d EB
E14
E14 4d atRA
E14 10d EB
H3K4me3
(scale -2 to 6)
H3K27me3
(scale -3 to 4)
TBP
(scale -2 to 3)
RNAPII
(scale -1 to 4)
H3K36me3
(scale -1 to 3)
Expression
(scale -2 to 7)
H3K9me2
(scale -3.5 to 2)
H3-Core
(scale -4 to 2)
Atrx
81
65
47
195
140
336
146
120

Fig S4c

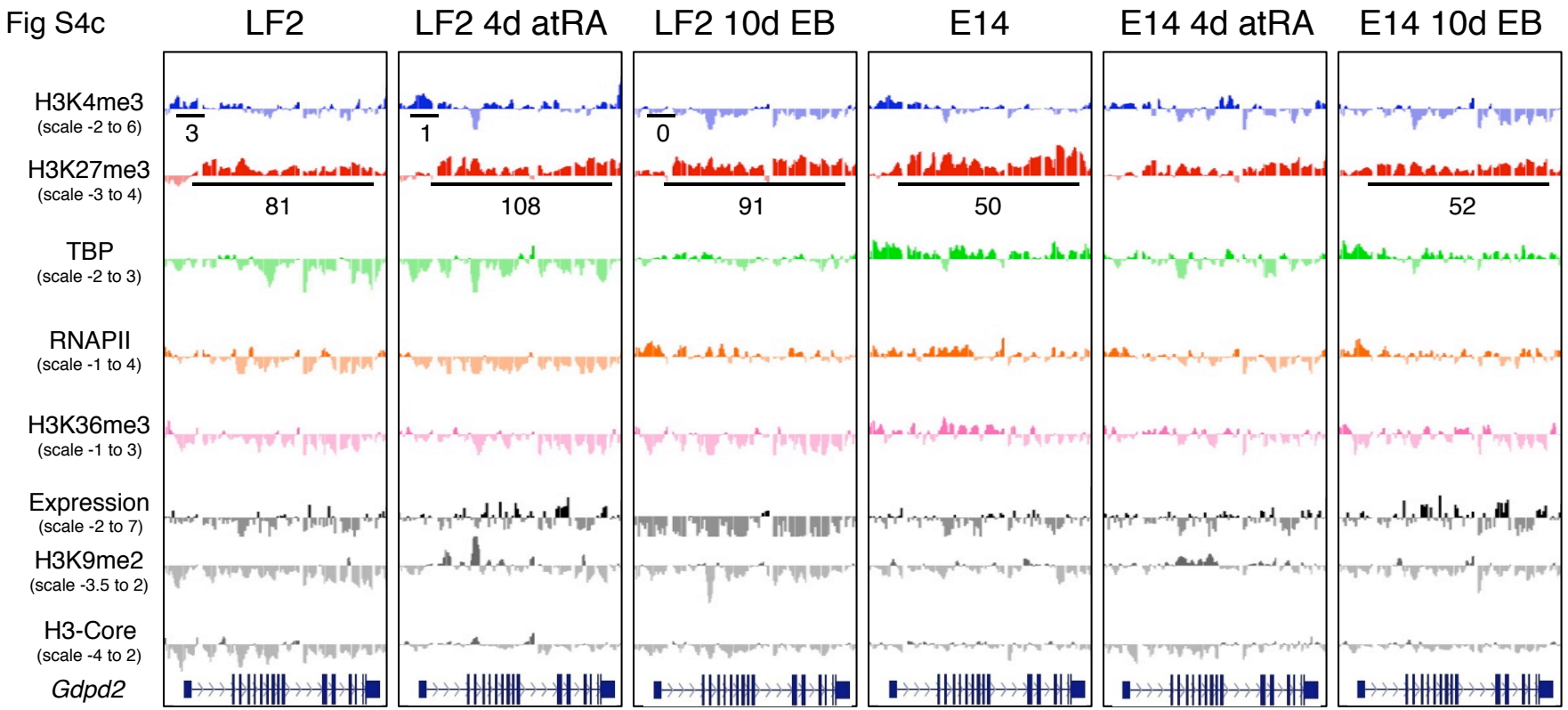
LF2
LF2 4d atRA
LF2 10d EB
E14
E14 4d atRA
E14 10d EB
H3K4me3
(scale -2 to 6)
H3K27me3
(scale -3 to 4)
TBP
(scale -2 to 3)
RNAPII
(scale -1 to 4)
H3K36me3
(scale -1 to 3)
Expression
(scale -2 to 7)
H3K9me2
(scale -3.5 to 2)
H3-Core
(scale -4 to 2)
Gdpd2
3
81
1
108
0
91
50
52

Supplemental figure 5

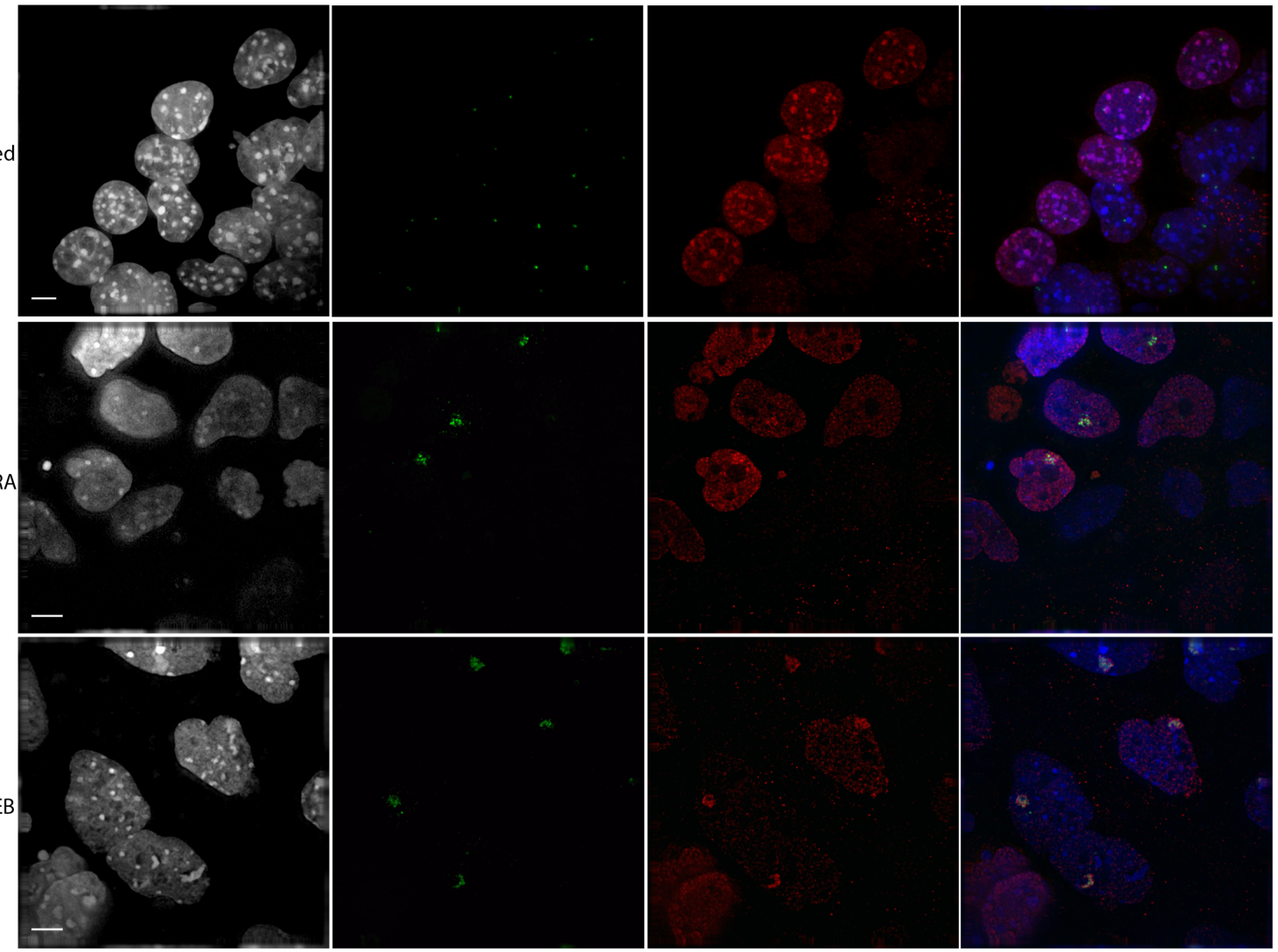

	% Nuclei *Xist*	% Nuclei H3K27me3 colocalizing with *Xist*	% Nuclei showing no signs of XCI
undifferentiated	0	0	100
4d atRA	33	17	67
10d EB	86	85	14

Supplemental figure 6

Fig S6a

H3K27me3 over the silent Aristaless related homeobox (*Arx*; chrX)

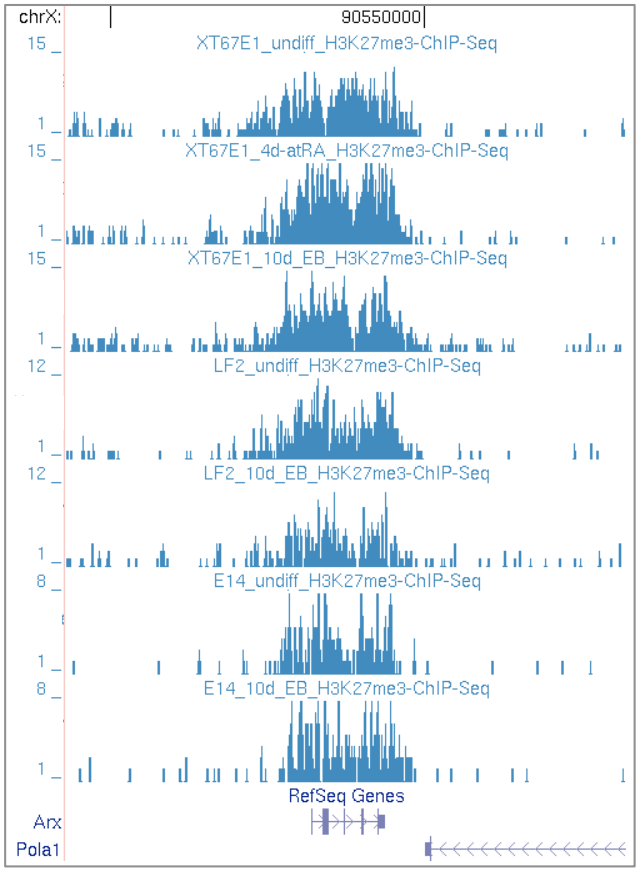

Fig S6b

H3K27me3 over the silent Androgen receptor (*Ar*; chrX)

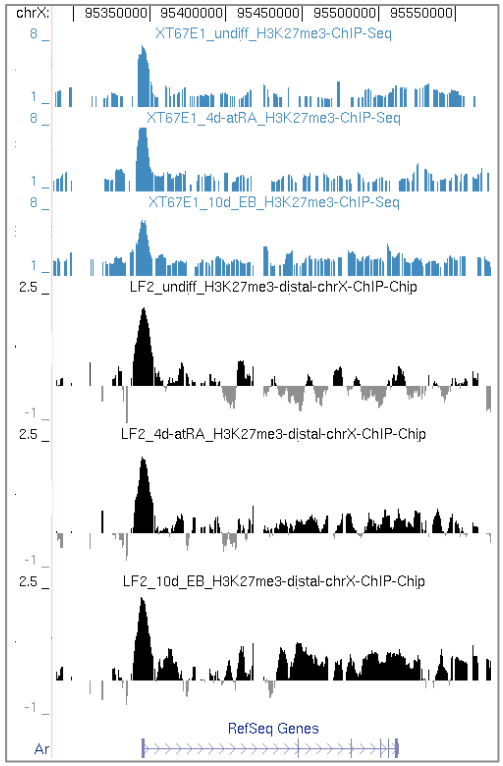

Fig S6c

H3K4me3 over the active *Pin4* and *Ercc6l* genes (chrX)

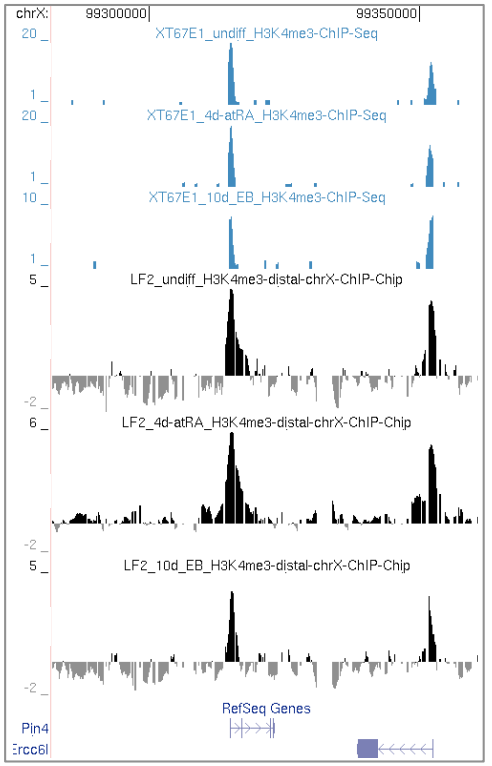

Supplemental figure 7

Fig S7a

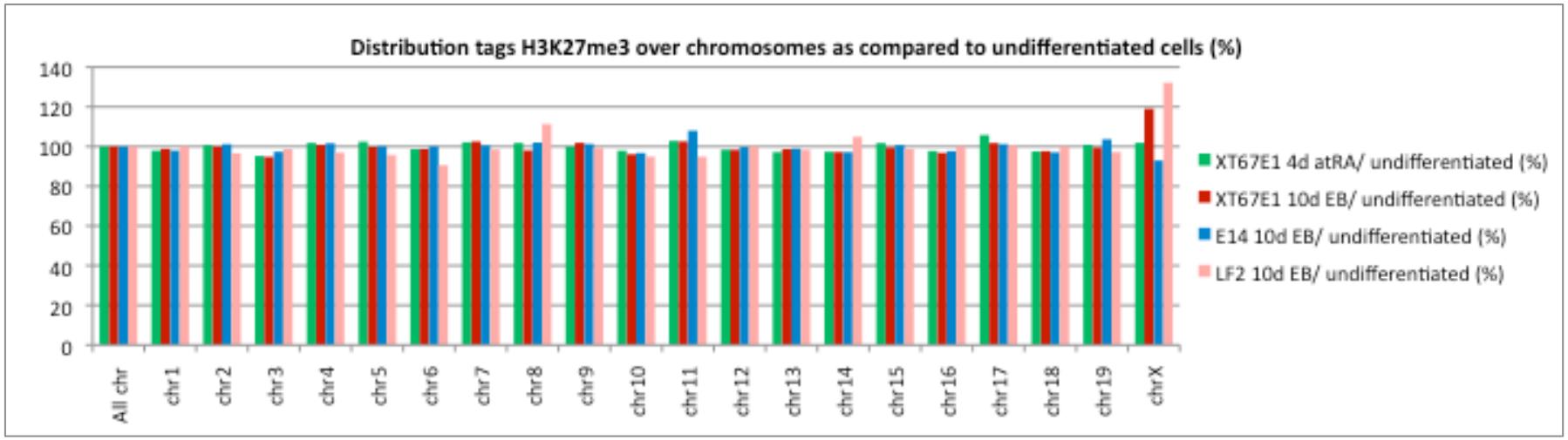

Fig S7b

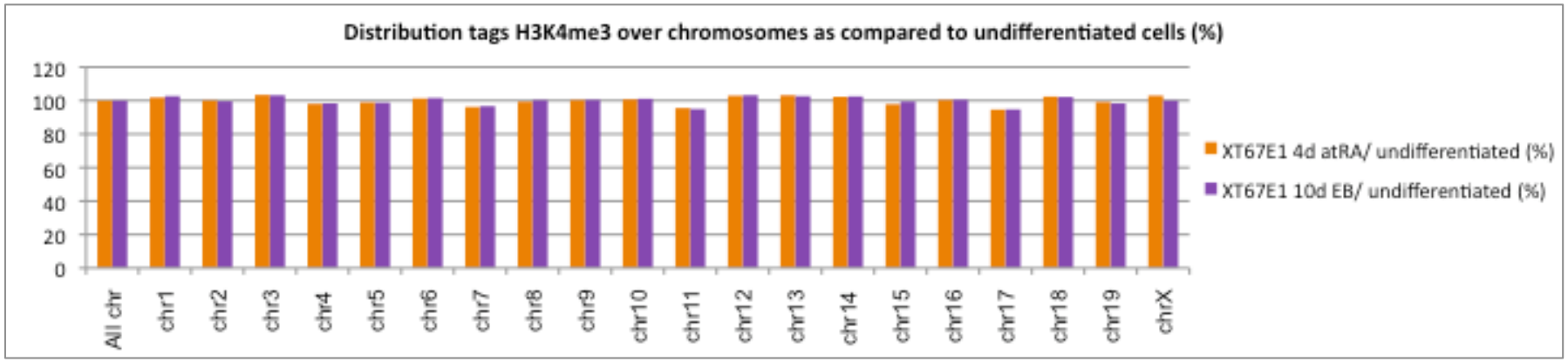

Supplemental figure 8

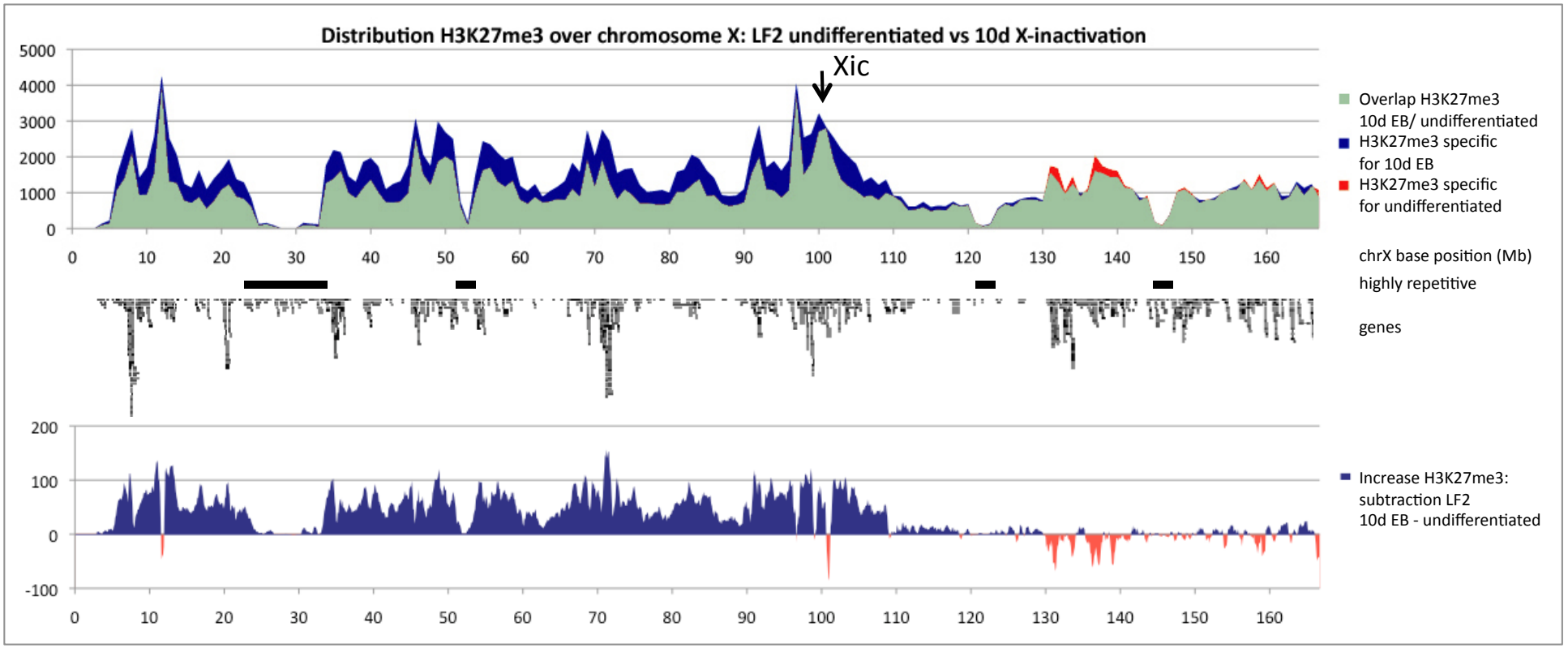

Supplemental figure 9

Fig S9a

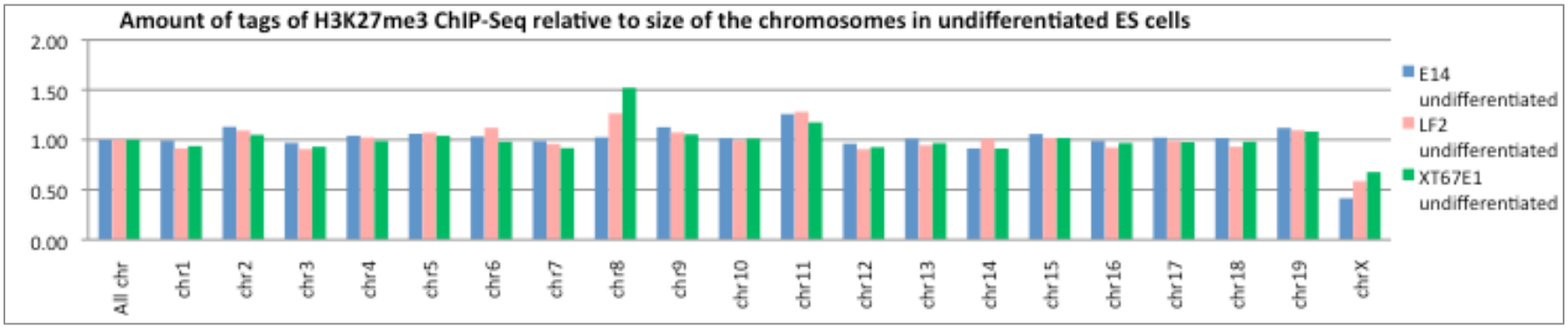

Fig S9b

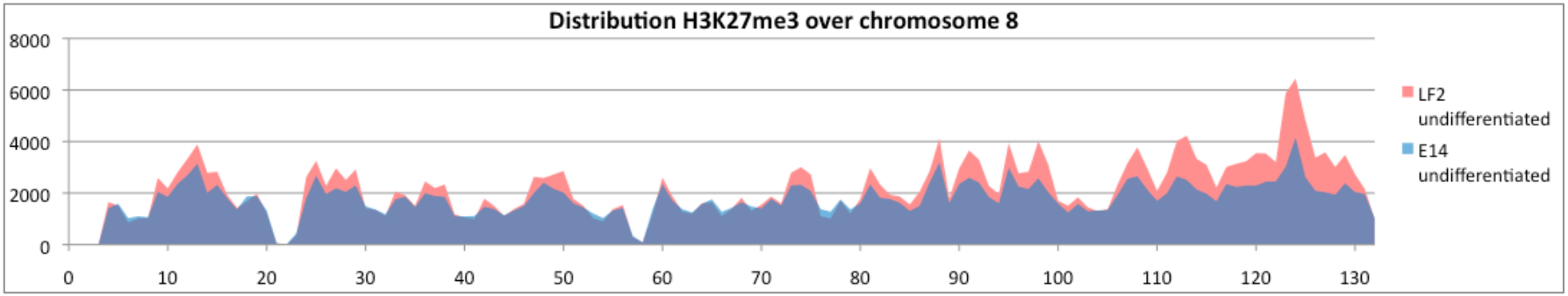

Fig S9c

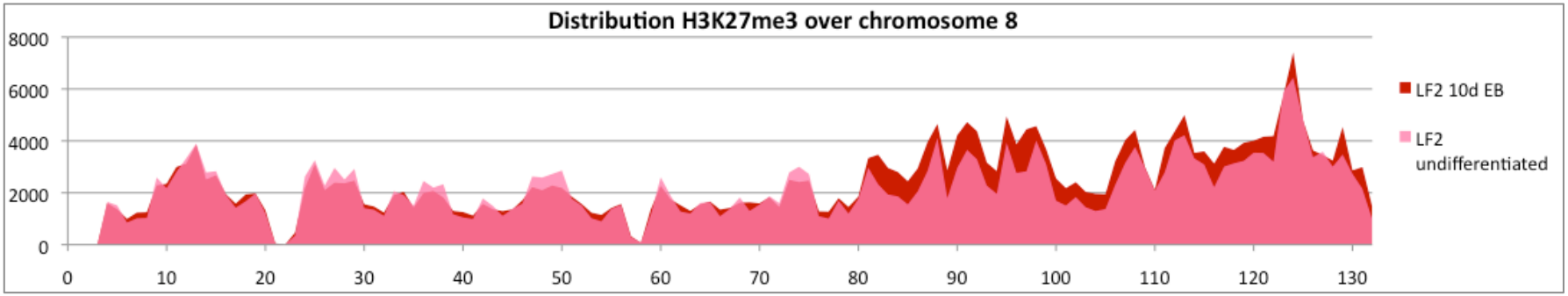

Fig S9d

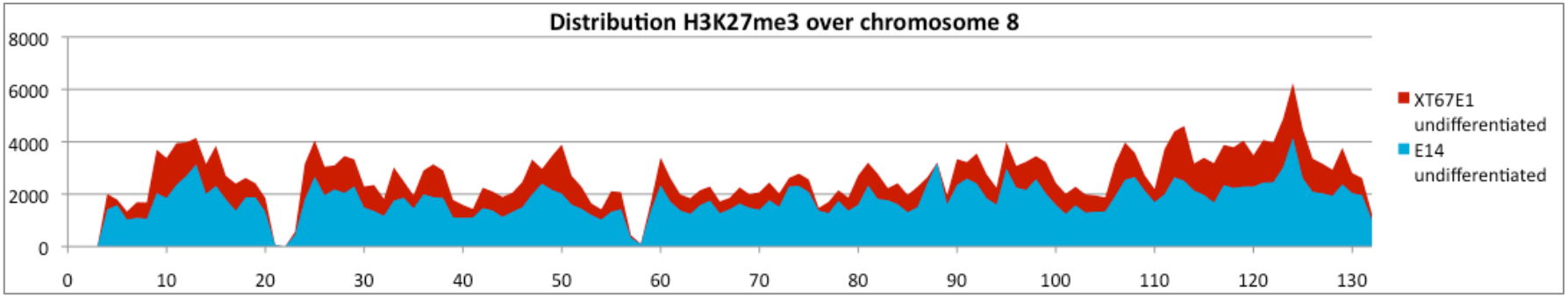

Supplemental figure 10

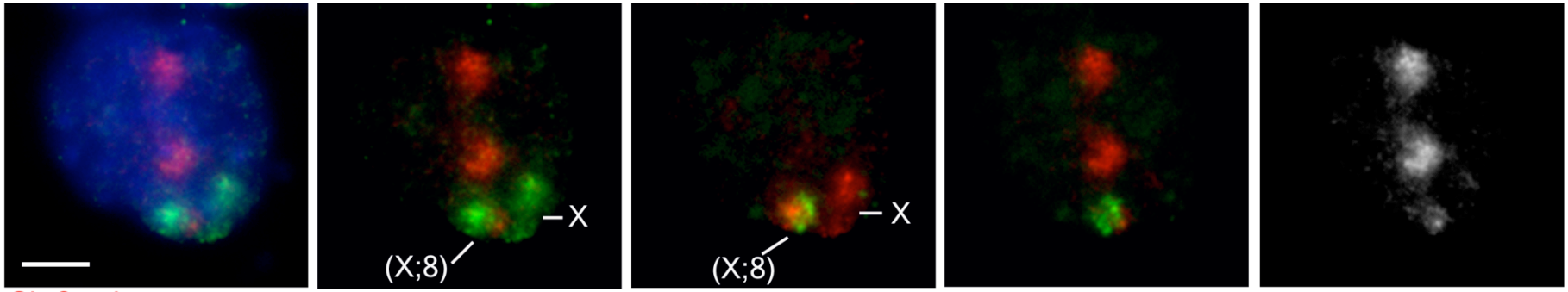

Chr8 paint
Xpaint

Chr8 paint
Xpaint

Xpaint
Xist

Chr8 paint
Xist

Chr 8 paint

Supplemental figure 11

H3K27me3 over the silent Meis homeobox 2 (*Meis2*; chr2)